

## Mimicking an Atomically Thin "Vacuum Spacer" to Measure the Hamaker Constant between Graphene Oxide and Silica

Chu, Liangyong; Korobko, A.V.; Cao, Anping; Sachdeva, Sumit; Liu, Zhen; de Smet, Louis C P M; Sudholter, E.J.R.; Picken, Stephen J.; Besseling, Nicolaas A M

**DOI**

[10.1002/admi.201600495](https://doi.org/10.1002/admi.201600495)

**Publication date**

2017

**Document Version**

Accepted author manuscript

**Published in**

Advanced Materials Interfaces

**Citation (APA)**

Chu, L., Korobko, A. V., Cao, A., Sachdeva, S., Liu, Z., de Smet, L. C. P. M., Sudholter, E. J. R., Picken, S. J., & Besseling, N. A. M. (2017). Mimicking an Atomically Thin "Vacuum Spacer" to Measure the Hamaker Constant between Graphene Oxide and Silica. *Advanced Materials Interfaces*, 4(5), 1-5. Article 1600495. <https://doi.org/10.1002/admi.201600495>

**Important note**

To cite this publication, please use the final published version (if applicable). Please check the document version above.

**Copyright**

Other than for strictly personal use, it is not permitted to download, forward or distribute the text or part of it, without the consent of the author(s) and/or copyright holder(s), unless the work is under an open content license such as Creative Commons.

**Takedown policy**

Please contact us and provide details if you believe this document breaches copyrights. We will remove access to the work immediately and investigate your claim.

DOI: 10.1002/((please add manuscript number))

**Article type: Communication**

**Mimicking an Atomically-thin 'Vacuum Spacer' to Measure the Hamaker Constant between Graphene Oxide and Silica**

*Liangyong Chu, Alexander V. Korobko, Anping Cao, Sumit Sachdeva, Zhen Liu, Louis C. P. M. de Smet, Ernst J. R. Sudhölter, Stephen J. Picken, Nicolaas A.M. Besseling\**

Liangyong Chu, Dr. Alexander V. Korobko, Anping Cao, Sumit Sachdeva, Dr. Zhen Liu, Dr. Louis C. P. M. de Smet, Prof. Ernst J. R. Sudhölter, Prof. Stephen J. Picken, Dr. Nicolaas A.M. Besseling  
Department of Chemical Engineering, Organic Materials & Interface (OMI), Delft University of Technology, Julianalaan 136, 2628 BL Delft, The Netherlands  
E-mail: N.A.M.Besseling@tudelft.nl

**Keywords:** Hamaker constant, vacuum spacer, 2-dimesional materials, graphene oxide, atomic force microscopy

In nanoscience, control of the separation between surfaces, with sub-nm accuracy, is often important. For instance, when studying Van der Waals (VdW) forces<sup>[1]</sup> or creating nanogaps for molecule detection and separation<sup>[2]</sup>. At nanometre scales, 1D or 3D spacers, such as nanotubes and nano-particles, are susceptible to deformation<sup>[3]</sup>. A 2D spacer is expected to yield a more accurately defined separation, owing to the high atom density and strength in planar direction. Herein, atomically thin 2D graphene oxide (GO) was used as nanometre-scale spacer with sub-nm accuracy, to study VdW interactions. However, using such a physical spacer introduces additional interactions, obscuring the interactions of interest. We demonstrate how these contributions can be eliminated by effectively mimicing the use of a 'vacuum spacer'. In this way, we obtain the effective Hamaker constant between GO and silica.

Following the excitement about graphene, GO is drawing more and more attention.<sup>[4]</sup> Using GO as a precursor, many graphene derivatives and heterostructures<sup>[1]</sup> have been made, and used in various areas such as composites,<sup>[5]</sup> energy storage and conversion,<sup>[6]</sup> bioscience, mechanical and electronic devices and sensors.<sup>[7]</sup>

1 In all these applications, graphene-based materials are used in combination with other  
2 materials. Hence, the relevance of interfacial forces such as VdW<sup>[1, 8]</sup>, capillary<sup>[9]</sup> and  
3 electrostatic<sup>[10]</sup> forces. The VdW forces, which are always present, can be quantified by the  
4 so-called Hamaker constant.<sup>[11]</sup> The unretarded VdW interaction energy  $U_{\text{VdW}}(d)$  between  
5 two material surfaces is<sup>[11, 12]</sup>

$$U_{\text{VdW}}(d) = -A_{12}/12\pi d^2 \quad (1)$$

14 where  $d$  is the separation distance, and  $A_{12}$  is the Hamaker constant.

17 Knowing the Hamaker constant between graphene-based materials and other materials (e.g.  
18 silicon (Si) with native silica layer as used in electronic devices) is important for their  
19 application, but measuring this constant is challenging. According to Equation 1, to determine  
20 the Hamaker constant, the VdW interaction energy needs to be determined for a known  
21 separation distance. Several investigations have been made to establish the strength of VdW  
22 interactions between graphene and Si by measuring the adhesion energy.<sup>[13]</sup> However, the  
23 effective distance between a graphene sheet and a Si surface could not be determined  
24 precisely in these experiments. The effective separation distance of two ‘touching’ surfaces  
25 varies from one to two Ångstroms depending on the surface roughness.<sup>[14]</sup> At small separation  
26 distances, the limited accuracy of the distance measurement (typical error of 1 nm) leads to a  
27 huge error in the calculated value of the Hamaker constant according to Equation 1. In  
28 principle, this problem could be solved by a spacer with a precisely known thickness of about  
29 1 nm. At such distances, the magnitude of the VdW energy is sufficient for accurate  
30 measurement, and the retardation effect is unimportant.<sup>[15]</sup> The ideal spacer would be one that  
31 ‘consists of vacuum’, so that it would not contribute to the interactions.

32 Capillary<sup>[9]</sup> and electrostatic<sup>[10]</sup> forces complicate determination of the VdW energy even  
33 further.

34 **Figure 1** illustrates the experiment that mimics the application of a vacuum spacer in an AFM  
35 force measurement, by measuring the adhesion force between an AFM tip and both mono-

1 and bi- layers of GO on a Si/polymer substrate. From the difference between the measured  
2 adhesion force on GO monolayer and on GO bilayer (Figure 1.a, b respectively), capillary and  
3 electrostatic forces, and the VdW interactions between tip and underlying substrate cancel.  
4

5 Hence, we obtain the interaction force between a levitating GO nanosheet and the AFM tip, at  
6 a distance  $d$  corresponding to the thickness of the GO top layer, as if they were separated by a  
7 vacuum spacer with a thickness equal to that of the intervening GO top layer.  
8

9 Sample preparation and morphology of the Si/PEI/GO structures depicted in Figure 1.a and b  
10 are summarised and illustrated in **Figure 2**, and described in the sample preparation section.  
11

12 The surface morphology of the Si/PEI/GO sample as drawn in Figure 2.c.5, was characterized  
13 using HybriD Mode AFM, by which we obtain simultaneously a height image and an  
14 adhesive-force image (for details see the *Instrumentation and methods* part). **Figure 3** shows  
15 results collected at different locations of the same sample. Height images are shown in Figure  
16 3.a, d. GO flakes are recognisable by their larger height, by about 5 nm, relative to the silicon.  
17

18 This 5 nm represents the combined thickness of GO and underlying PEI. Features in the  
19 adhesion-force image coincide with features in the height counterpart. However, inspection of  
20 the adhesion-force image reveals features not visible in the height image. Folding and  
21 overlapping of GO, which forms a bilayer at some places, causes variations of the adhesion  
22 force. In adhesion-force images (Figure 3.b, 2.e) and profiles (Figure 3.c, 3.f) we recognise  
23 two distinct levels at the GO flakes. In Figure 3.d and 3.e we observe a straight edge, quite  
24 different from other more irregular edges of the GO flakes, which represents a fold of a flake.  
25

26 Adjoining this edge there must be a GO bilayer. Indeed, in the adhesion-force image (Figure  
27 3e), and profile (Figure 3f), we clearly recognise the bilayer patch adjoining this fold. The  
28 bilayer is characterised by a larger adhesive energy than the monolayer patches. Also in other  
29 places (e.g. image 2.b and profile 2.c) we recognise patches with this higher-level adhesive  
30 force. After the tape treatment, both the GO monolayer and bilayer are rough. For the  
31 subsequent analysis, we selected regions on the monolayer and on the bilayer where the  
32

height is the same. This procedure is explained in detail in part 3 of the supporting information. Figure 3.c and f represent typical single scan profiles along the white lines in Figure 3.a, 3.b and 3.d, 3e respectively.

According to the Derjaguin approximation<sup>[16]</sup>, the interaction force  $F$  between a spherical surface of radius  $R$  (e.g. the AFM tip) and a flat surface (e.g. the Si/PEI/GO surface) is related to the interaction energy per unit area  $U$  between two planar surfaces via

$$\frac{F}{R} = 2\pi U \quad (2)$$

This relation applies to e.g. the VdW interactions and screened electrostatic interactions when the distance between the surfaces is considerably smaller than the radius  $R$ . It does not apply to interactions associated with capillary bridges. According to the Hamaker-de Boer approximation,<sup>[11, 17]</sup> the VdW interaction energy per unit area between a planar silica surface and a Si/PEI/GO surface at a distance  $D$ , with a GO thickness  $h_G$  and a PEI thickness  $h_P$ , is described by:

$$U_{\text{VdW}}(D, h_G, h_P) = -\left[ \frac{A_{\text{SG}}}{12\pi} \left( \frac{1}{D^2} - \frac{1}{(D + h_G)^2} \right) + \frac{A_{\text{SP}}}{12\pi} \left( \frac{1}{(D + h_G)^2} - \frac{1}{(D + h_G + h_P)^2} \right) + \frac{A_{\text{SSi}}}{12\pi} \left( \frac{1}{(D + h_G + h_P)^2} \right) \right] \quad (3)$$

where  $A_{\text{SG}}$ ,  $A_{\text{SP}}$ ,  $A_{\text{SSi}}$  are the Hamaker constants of Silica/GO, Silica/PEI and Silica/Si, respectively (supporting information, part 1).

The capillary force ( $\frac{F}{R} \approx \sigma$ , the surface tension of water)<sup>[18]</sup> has a similar order of magnitude as the measured normalized force. However, its exact value is difficult to establish as it depends on humidity and the local surface morphology. Furthermore, the electrostatic force depends on the physical and chemical properties of the surface such as the surface charge densities, which are not known.

Assuming additivity, the measured normalized force  $F/R$  is

$$F/R = 2\pi U_{vdW}(D, h_G, h_P) + F_c/R + F_e/R \quad (4)$$

where  $F_c$  and  $F_e$  represent the capillary and electrostatic forces, respectively.

It is not possible to obtain the Hamaker constant  $A_{SG}$  using separate values for  $F_M/R$  or for  $F_B/R$  as reported in Figure 3, because there are four unknown variables ( $A_{SG}$ ,  $D$ ,  $F_c$ ,  $F_e$ ). In order to obtain the Hamaker constant, the capillary and electrostatic forces have to be eliminated from analysis. Making some reasonable assumptions, it is possible to obtain the Hamaker constant from the difference between  $F_M/R$  and  $F_B/R$ . These assumptions are the additivity principle (Equation 4), and the assumption that the electrostatic and capillary forces are the same for GO monolayers and GO bilayers. This is reasonable as these contributions are largely determined by the nature of the outer surface, which is the same for GO mono and bilayers.

The capillary force  $F_c$  in AFM force measurement can be described as,<sup>[19]</sup>  $F_c = 2\pi\gamma R(\cos\theta_1 + \cos\theta_2)$ , where  $\gamma$  is surface tension of water,  $R$  is the radius of the AFM tip,  $\theta_1$  is the contact angle of AFM tip(silica),  $\theta_2$  is the contact angle of sample surface. The folded under layer has very limited effect on  $\theta_2$ . The effect on the capillary force itself is even smaller.

The plasma treatment of the GO surfaces will probably induce some changes. However, this does not influence our final result, as the upper layer does not contribute to the final results and acts as a protecting layer for the second layer during the plasma treatment.

According to these assumptions, the normalised force for a levitating GO nanosheet positioned below the AFM tip at a distance  $d$  corresponding to the thickness of the GO top layer, equals

$$\begin{aligned} F_B/R - F_M/R &= [2\pi U(D, 2h_G, h_{PB}) + F_{B,c} + F_{B,e}] - [2\pi U(D, h_G, h_{PM}) + F_{M,c} + F_{M,e}] \\ &= \frac{A_{SG}-A_{SP}}{6} \left( \frac{1}{h_G^2} - \frac{1}{(2h_G)^2} \right) \\ &= \frac{1}{8} \frac{A_{SG}-A_{SP}}{d^2} \end{aligned} \quad (5)$$

Here, the separation distance  $d$  is equal to  $h_G$ . The second equality assumes that capillary and electrostatic forces are the same for the GO mono- and bilayer, so that these cancel. This relation enables us to calculate  $A_{SG}$  from the force difference, once  $R$ ,  $d$  and  $A_{SP}$  are known. The value for  $d = h_G$  is  $0.89 \pm 0.06 \text{ nm}$  (supporting information part 4). The radius  $R$  of the AFM tip is  $10.6 \text{ nm}$  (supporting information part 6). To estimate  $A_{SP}$  we refer to Berthelot principle<sup>[16]</sup>

$$A_{SP} \approx (A_{SS}A_{PP})^{1/2} \quad (6)$$

For polymers such as e.g. PEI, the Hamaker constant is smaller than  $16 k_B T$ , that of water is  $10 k_B T$ . Thus, for  $A_{PP}$  the Hamaker constant of the hydrated PEI/PEI layer we use the value  $13 \pm 3 k_B T$ .<sup>[16]</sup>  $A_{SS}$ , the Hamaker constant of Silica/Silica equals  $16.09 k_B T$ .<sup>[20]</sup> All Hamaker constants are expressed in units of  $k_B T$  at room temperature ( $4.07 \times 10^{-21} \text{ J}$ ).

Using the measured value for the force difference of  $75 \pm 5 \text{ mN/m}$  (see Figure 3 and supporting information part 3), equations (5) and (6) yield the value of the Hamaker constant of GO/Silica of  $124.6 \pm 16.6 k_B T$  (supporting information 7). This result is well reproduced when choosing different locations on the sample and when doing the experiment at different temperature and humidity as demonstrated in Figure 3(d-f).

As a conclusion, on one hand, we found that 2D materials can be used as a nanometre-scale spacer, with sub-nm accuracy. On the other hand, we demonstrated that mimicking a ‘vacuum spacer’ is possible in AFM force measurements. This leads to an accurate determination of the Hamaker constant between GO and silica, which is crucial to many GO based applications. This ‘vacuum-spacer method’, that was in this paper applied to GO, can in principle be applied to other 2D materials as well. We believe that this will open new applications of 2D materials in nanoscience and nanotechnology.

## Experimental Section

### *Chemicals and materials*

1 Graphene oxide (GO), synthesized using Hummer's method, was purchased from Graphene  
2 Supermarket. The elemental composition of GO was characterized using X-ray photoelectron  
3 spectroscopy (XPS) (supporting information 5). A stable dispersion of 0.5 g GO in 1 L Milli-  
4 Q water was prepared using ultrasonication for 1 h, using an USC-TH ultrasonic bath from  
5 VWR Scientific. The dispersion was then centrifugation at 4000 rpm for 1 h, using a  
6  
7  
8  
9  
10  
11  
12  
13  
14  
15  
16  
17  
18  
19  
20  
21  
22  
23  
24  
25  
26  
27  
28  
29  
30  
31  
32  
33  
34  
35  
36  
37  
38  
39  
40  
41  
42  
43  
44  
45  
46  
47  
48  
49  
50  
51  
52  
53  
54  
55  
56  
57  
58  
59  
60  
61  
62  
63  
64  
65

Graphene oxide (GO), synthesized using Hummer's method, was purchased from Graphene Supermarket. The elemental composition of GO was characterized using X-ray photoelectron spectroscopy (XPS) (supporting information 5). A stable dispersion of 0.5 g GO in 1 L Milli-Q water was prepared using ultrasonication for 1 h, using an USC-TH ultrasonic bath from VWR Scientific. The dispersion was then centrifugation at 4000 rpm for 1 h, using a Megafuge 2.0R centrifuge from Heraeus Instruments with rotor radius of 20 cm. The supernatant was decanted and used for the sample preparation. Polyethylenimine (PEI,  $M_w = 25000$  g/mol) was purchased from Sigma-Aldrich and used as received. A 0.1 g/L PEI aqueous solution was prepared using milli-Q water. A chip of about of 1 cm  $\times$  1 cm was cut from a (100) Silicon wafer with a native oxide layer of about 2 nm obtained from Sil'Tronix Silicon Technologies. The silicon chip was first rinsed with demi-water and ethanol followed by sonication using ethanol and acetone for 5 minutes, respectively. Plasma treatments of samples were performed with oxygen plasma for 1 minute at a pressure of 1600 mTorr using a Harrick plasma cleaner (Anadis Instruments). After plasma treatment, the silicon wafer was stored in milli-Q water for more than 24 hours to equilibrate.

### *Sample preparation*

The Si surface was coated with a monolayer of Polyethylenimine (PEI) by dipping the Si chip in an aqueous PEI solution (0.1 g/L) for 15 min. The sample was then rinsed in milli-Q water for 5 min to remove non-adsorbed PEI. Subsequent coating by GO was done by immersing the sample for 15 min in the aqueous GO dispersion prepared as described above. To remove excess GO, the sample was dipped in milli-Q water for 5 min. Due to carboxyl groups, GO is negatively charged and adsorbs at the positively charged PEI layer. All these steps in the sample preparation were done whilst the solution was stirred.

After deposition, a tape treatment was performed. The tape was pressed onto the sample using a finger as shown in inset of Fig 2b, and then torn off. To remove the polymer (PEI and/or

1 residue of the tape treatment, the sample was treated with oxygen plasma for 1 min. This  
2 completes the sample preparation.

### 3 4 *Instrumentation and methods*

5  
6 A NTEGRA AFM instrument from NT-MDT was used in all AFM experiments. High  
7 sensitivity measurements were performed using the ‘HybriD Mode’ method, developed and  
8 implemented by NT-MDT. This method combines height imaging and tip-sample force  
9 tracking simultaneously.<sup>29</sup> With hybrid mode AFM, a vertical oscillation of the sample is  
10 implemented at frequencies well below the resonances of the probe and the piezo-element to  
11 improve the signal to noise ratio. In the HybriD Mode method, at each point the tip performs a  
12 cycle of approaching and retracting. The range of approaching and retracting was set at 20 nm.  
13 In the approaching phase, the tip goes from non-touching to the touching regime, and the  
14 deflection signal of the cantilever records the force that the tip experiences. In the retracting  
15 phase of the cycle, the tip experiences strong adhesive interactions reflected by a jump by  
16 which the tip detaches. The latter jump is proportional to the magnitude of the adhesive force  
17  $F$ . As a result, we obtain the surface morphology height image as well as the normalized  
18 adhesion-force image at the same time.  
19  
20  
21  
22  
23  
24  
25  
26  
27  
28  
29  
30  
31  
32  
33  
34  
35  
36

37  
38 A NSG 03 silicon tip purchased from NT-MDT, with nominal value for the tip radius of 7 nm  
39 (guaranteed < 10 nm) and a nominal spring constant of 0.4 - 2.7 N/m was used with the  
40 hybrid mode measurements. Using high-resolution SEM, we determined that the tip radius  
41 equals 10.6 nm (supporting information 6). The actual value of the spring constant was  
42 measured using the thermal noise method.<sup>30</sup> Scanning the surface morphology, 512 x 512  
43 points are recorded in 4  $\mu\text{m}$  x 4  $\mu\text{m}$  area. HA\_NC AFM probes from NT-MDT with a silicon  
44 tip radii of about 10 nm were used for the standard tapping mode height scanning. The  
45 HybriD Mode images and standard tapping mode height images were all scanned with a rate  
46 of 0.5 Hz.  
47  
48  
49  
50  
51  
52  
53  
54  
55  
56  
57  
58  
59  
60  
61  
62  
63  
64  
65

## Supporting Information

Supporting Information is available from the Wiley Online Library or from the author.

## Acknowledgements

We acknowledge the PhD Scholarship of Liangyong Chu from China Scholarship Council of the Ministry of Education of China. We acknowledge Marcel Bus for the assistance with the AFM instruments.

Received: ((will be filled in by the editorial staff))

Revised: ((will be filled in by the editorial staff))

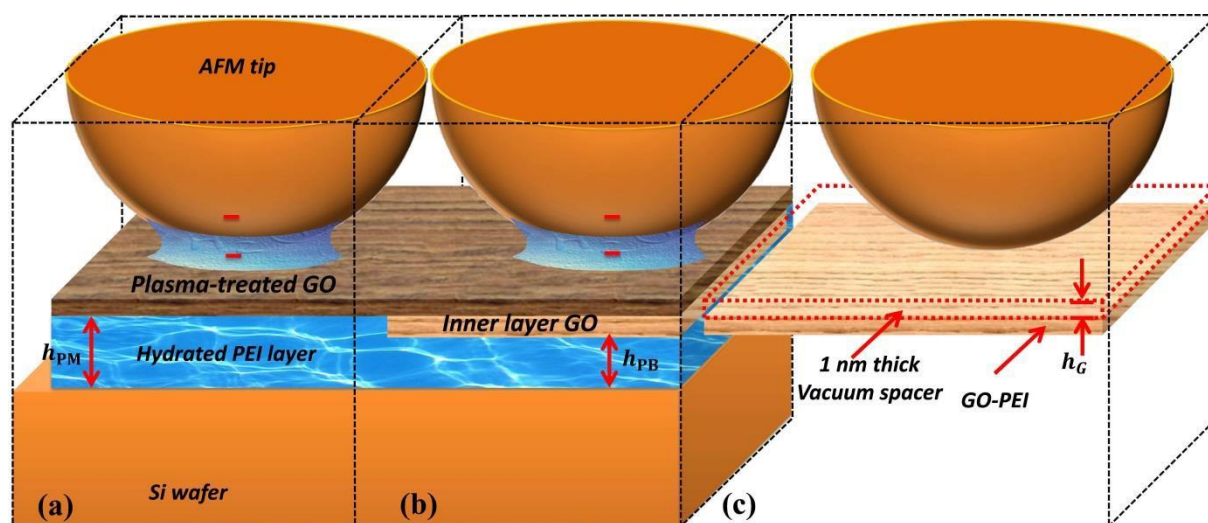
Published online: ((will be filled in by the editorial staff))

- [1] A. K. Geim, I. V. Grigorieva, *Nature* 2013, 499, 419.
- [2] D. R. Ward, N. K. Grady, C. S. Levin, N. J. Halas, Y. Wu, P. Nordlander, D. Natelson, *Nano letters* 2007, 7, 1396; D.-K. Lim, K.-S. Jeon, H. M. Kim, J.-M. Nam, Y. D. Suh, *Nature materials* 2010, 9, 60; H. Li, Z. Song, X. Zhang, Y. Huang, S. Li, Y. Mao, H. J. Ploehn, Y. Bao, M. Yu, *Science* 2013, 342, 95.
- [3] J. Sun, L. He, Y.-C. Lo, T. Xu, H. Bi, L. Sun, Z. Zhang, S. X. Mao, J. Li, *Nature materials* 2014, 13, 1007.
- [4] K. S. Novoselov, A. K. Geim, S. Morozov, D. Jiang, Y. Zhang, S. Dubonos, I. Grigorieva, A. Firsov, *science* 2004, 306, 666.
- [5] S. Stankovich, D. A. Dikin, G. H. Dommett, K. M. Kohlhaas, E. J. Zimney, E. A. Stach, R. D. Piner, S. T. Nguyen, R. S. Ruoff, *Nature* 2006, 442, 282; T. Ramanathan, A. Abdala, S. Stankovich, D. Dikin, M. Herrera-Alonso, R. Piner, D. Adamson, H. Schniepp, X. Chen, R. Ruoff, *Nature nanotechnology* 2008, 3, 327; T. Kuilla, S. Bhadra, D. Yao, N. H. Kim, S. Bose, J. H. Lee, *Progress in polymer science* 2010, 35, 1350.
- [6] G. Eda, G. Fanchini, M. Chhowalla, *Nature nanotechnology* 2008, 3, 270.
- [7] A. Das, S. Pisana, B. Chakraborty, S. Piscanec, S. Saha, U. Waghmare, K. Novoselov, H. Krishnamurthy, A. Geim, A. Ferrari, *Nature nanotechnology* 2008, 3, 210; F. Schedin, A. Geim, S. Morozov, E. Hill, P. Blake, M. Katsnelson, K. Novoselov, *Nature materials* 2007, 6, 652.
- [8] S. F. Shi, F. Wang, *Nature Nanotechnology* 2014, 9, 664.
- [9] Y. Li, Y. Wu, *Journal of the American Chemical Society* 2009, 131, 5851.
- [10] D. R. Dreyer, S. Park, C. W. Bielawski, R. S. Ruoff, *Chemical Society Reviews* 2010, 39, 228.
- [11] H. Hamaker, *physica* 1937, 4, 1058.
- [12] J. Visser, *Advances in Colloid and Interface Science* 1972, 3, 331.
- [13] S. P. Koenig, N. G. Boddeti, M. L. Dunn, J. S. Bunch, *Nature nanotechnology*, 6, 543; S. R. Na, J. W. Suk, R. S. Ruoff, R. Huang, K. M. Liechti, *Acs Nano* 2014, 8, 11234.
- [14] J. Rafiee, X. Mi, H. Gullapalli, A. V. Thomas, F. Yavari, Y. Shi, P. M. Ajayan, N. A. Koratkar, *Nature Materials* 2012, 11, 217.
- [15] J. Gregory, *Journal of Colloid and Interface Science* 1981, 83, 138.
- [16] J. Lyklema, 1991.
- [17] H. Hamaker, *Recueil des travaux chimiques des pays-bas* 1936, 55, 1015; H. Hamaker, *Recueil des travaux chimiques des pays-bas* 1937, 56, 3; J. De Boer, *Transactions of the Faraday Society* 1936, 32, 10.
- [18] S. Saito, T. Motokado, K. J. Obata, K. Takahashi, *Applied Physics Letters* 2005, 87, 234103.

- [19] X. Xiao, L. Qian, *Langmuir* 2000, 16, 8153.  
 [20] R. Hunter, *New York* 1987, 244.

**Figure 1.**

Schematic illustration of the experiment. (a) Silicon tip in contact with Si/PEI/GO monolayer. (b) Si tip in contact with Si/PEI/GO bilayer. The measured adhesion forces between the Si tip and the Si/PEI/GO layer in (a) and (b) are due to VdW forces, capillary forces, electrostatic forces and specific interactions between chemical moieties such as hydrogen bonds. (c) The difference between situation (a) and (b) mimics the AFM tip interacting with a GO monolayer in vacuum at a distance  $d$ , equal to the thickness of a GO monolayer. Capillary, electrostatic, and other forces cancel out.



1  
2  
3  
4  
5  
6  
7  
8  
9  
10  
11  
12  
13  
14  
15  
16  
17  
18  
19  
20  
21  
22  
23  
24  
25  
26  
27  
28  
29  
30  
31  
32  
33  
34  
35  
36  
37  
38  
39  
40  
41  
42  
43  
44  
45  
46  
47  
48  
49  
50  
51  
52  
53  
54  
55  
56  
57  
58  
59  
60  
61  
62  
63  
64  
65

**Figure 2.**

1  
2 (a) AFM height images of GO deposited on a Si/PEI surface. GO flakes are clearly visible  
3  
4 with thickness of about 1 nm,<sup>[28]</sup> as well as areas exhibiting a 2-fold increase of the height.  
5  
6 The latter is interpreted as two GO nanosheets overlapping (indicated by the green circle). (b)  
7  
8 AFM height images of the Si/PEI/GO sample after tape treatment. The inset of 2.b shows the  
9  
10 sample being pressed on the tape. (c) Schematic illustration of the sample preparation. Clearly,  
11  
12 GO flakes have remained at the sample upon the tape treatment. Their height increased to 4  
13  
14 nm, the heights for monolayer and bilayer sections are now the same. Furthermore, the  
15  
16 surface roughness increased. There are two possible explanations for the increased height of  
17  
18 the GO-covered regions: (c.3) the tape/PEI interaction is so strong that (part of) the PEI next  
19  
20 to GO flakes was removed by the tape, and the tape/GO interaction is so much weaker that  
21  
22 GO and PEI covered by it were not removed. (c.4) polymer molecules from the tape were left  
23  
24 behind, and their quantity on GO was larger than that on PEI. After plasma treatment, the  
25  
26 sample has flakes of GO with PEI underneath on Si. The area not covered by GO is simply  
27  
28 bare Si, as illustrated in (c.5). As discussed in detail, this structure is confirmed by AFM  
29  
30 height and force images, simultaneously obtained by the HybriD Mode method.<sup>[29]</sup>  
31  
32  
33  
34  
35  
36  
37  
38  
39  
40  
41  
42  
43  
44  
45  
46  
47  
48  
49  
50  
51  
52  
53  
54  
55  
56  
57  
58  
59  
60  
61  
62  
63  
64  
65

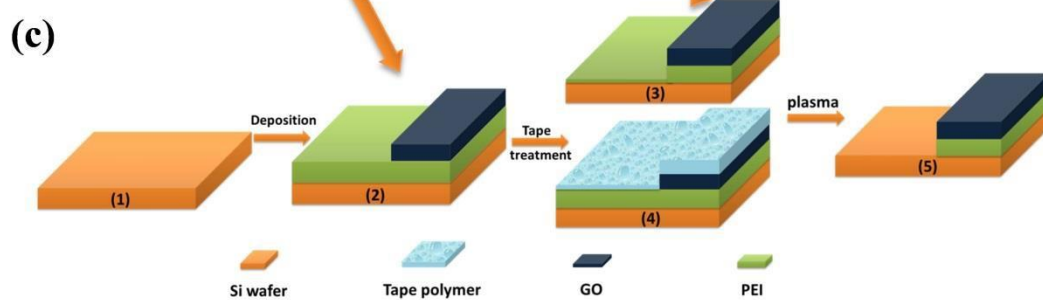
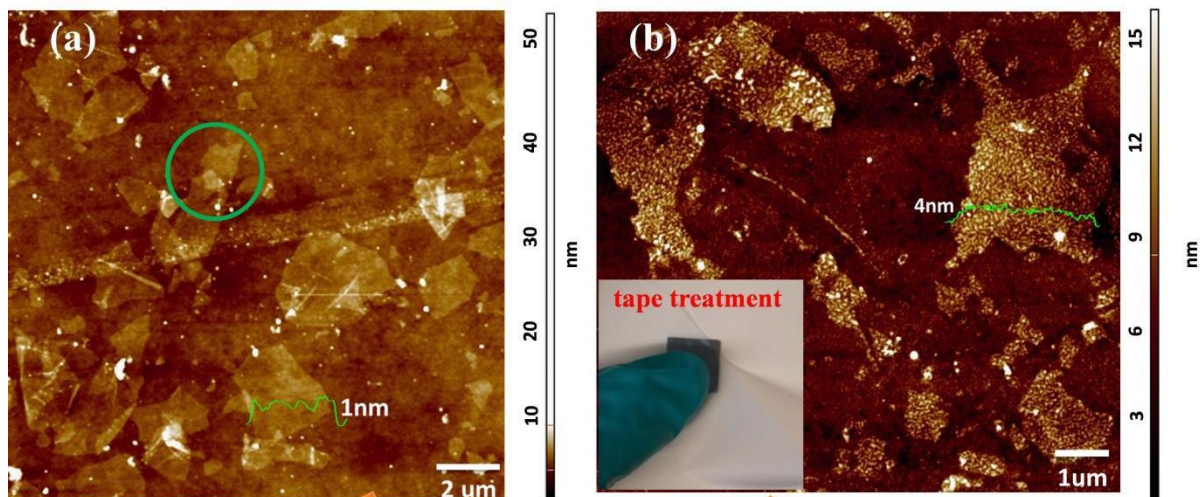
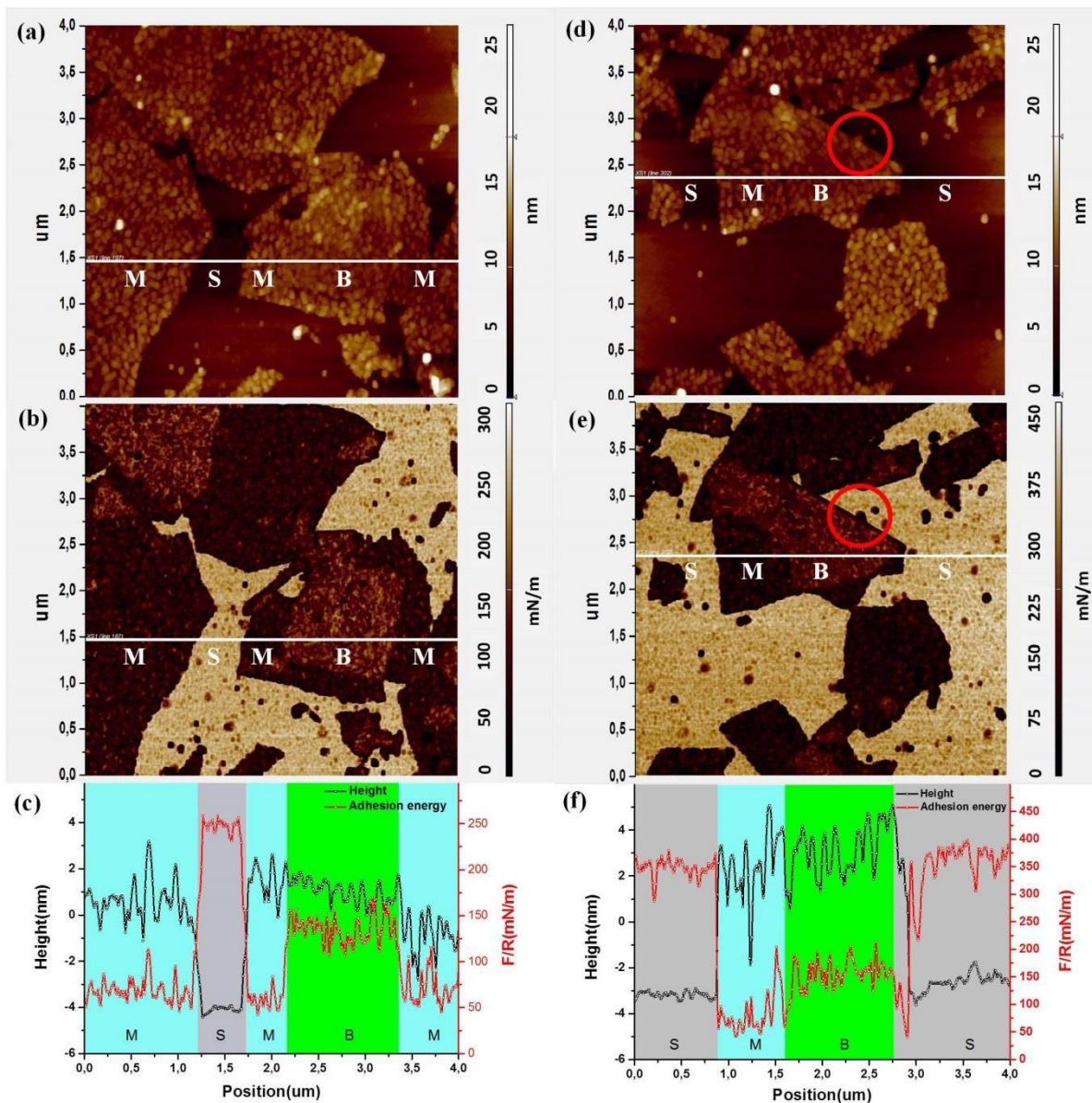


**Figure 3.**

Surface morphology and adhesion-force images and profiles of Si/PEI/GO samples with a structure as illustrated in Fig. 2.5, obtained using HybriD Mode AFM. (a) Height image. (b) Normalized adhesion-force image of the same area. (c) Height and normalized adhesion-force profiles along the white line indicated in (a) and (b). S marks bare Si, M marks PEI/monolayer GO on Si wafer, and B marks PEI/bilayer GO on Si wafer. Values of normalised adhesion forces averaged over 5 points at a GO monolayer and at a bilayer are  $F_M/R = 76 \pm 3 \text{ mN/m}$  and  $F_B/R = 151 \pm 4 \text{ mN/m}$ , respectively, and the difference between these is  $75 \pm 5 \text{ mN/m}$ . (d) to (f) show the results of a repeated experiment at a different location of the same sample using the same AFM tip. These were obtained on another day, when temperature and humidity were somewhat different. Values  $F_M/R = 63 \pm 2 \text{ mN/m}$  and  $F_B/R = 136 \pm 3 \text{ mN/m}$  are quite different from the ones mentioned before, but the difference between these is the same within experimental accuracy ( $73 \pm 4 \text{ mN/m}$ ). The straight edge, indicated by the red circles represent a fold of the GO flake.



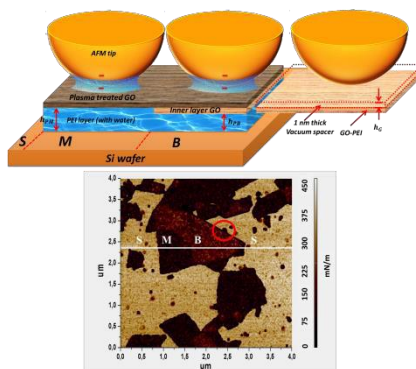
1  
2  
3  
4  
5 **The Hamaker constant between graphene oxide and silica**, which quantifies the strength  
6 of Van der Waals forces is determined, by mimicking a ‘vacuum spacer’ in an AFM force  
7 study. It is demonstrated that, a 2D spacer is expected to yield an accurately defined  
8 separation, owing to the high atom density and strength in planar direction compared with  
9 other dimensional spacers.

10  
11  
12 **Keyword:** Hamaker constant, vacuum spacer, 2-dimesional materials, graphene oxide, atomic  
13 force microscopy

14  
15  
16  
17  
18 Liangyong Chu, Alexander V. Korobko, Anping Cao, Sumit Sachdeva, Zhen Liu, Louis C. P.  
19 M. de Smet, Ernst J. R. Sudhölter, Stephen J. Picken, Nicolaas A.M. Besseling\*

20  
21  
22  
23  
24  
25 **Mimicking an Atomically-thin 'Vacuum Spacer' to Measure the Hamaker Constant  
26 between Graphene Oxide and Silica**

27  
28  
29 ToC Figure



## Supporting Information

## Mimicking an Atomically-thin 'Vacuum Spacer' to Measure the Hamaker Constant between Graphene Oxide and Silica

Liangyong Chu, Alexander V. Korobko, Anping Cao, Sumit Sachdeva, Zhen Liu, Louis C. P. M. de Smet, Ernst J. R. Sudhölter, Stephen J. Picken, Nicolaas A.M. Besseling\*

## 1. Deduction of the Hamaker constant of Graphene oxide

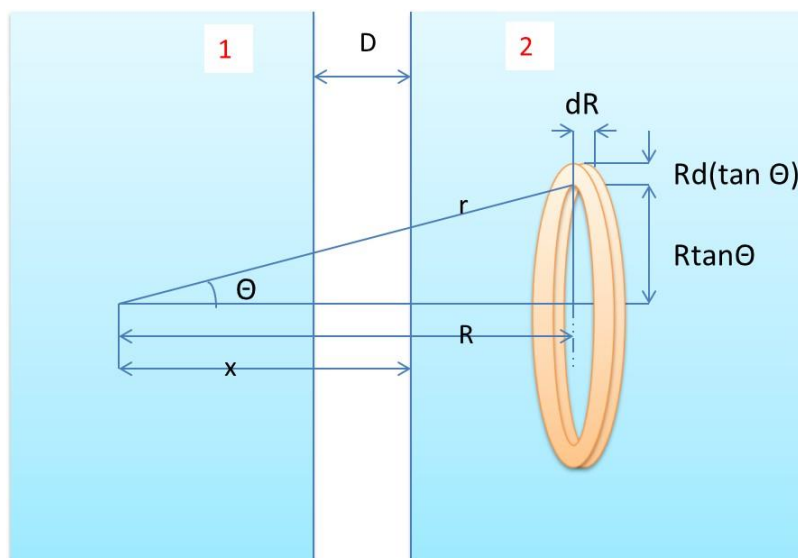


Fig S1. Derivation of the VdW interaction between flat surfaces, of two half-infinite bodies labelled phase 1 and 2.

According to the Hamaker-de Boer theory<sup>[1]</sup>, the VdW interaction energy between two parallel surfaces of half-infinite bodies (see Fig. S1) can be calculated as follows<sup>[2]</sup>:

Firstly, the interaction between a single element in phase 1 and the whole phase 2 is calculated,

$$u_{1,\text{phase2}} = - \int_x^\infty \int_0^\infty \frac{\beta_{12}\pi\rho_{N2}R^2(d\tan\theta^2)dR}{r^6}$$

$$\begin{aligned}
 &= -\pi\beta_{12}\rho_{N2} \int_x^\infty \int_0^\infty \frac{d(\tan\theta^2)dR}{R^4(\tan\theta^2+1)^3} \\
 &= -\frac{\pi\beta_{12}\rho_{N2}}{6} \frac{1}{x^3}
 \end{aligned} \tag{S1}$$

Where  $-\frac{\beta_{12}}{6r}$  describes the attractive energy between an element from phase 1 and one from phase 2, at a distance  $r$ . The parameter  $\beta_{12}$ , quantifying the strength of the interaction, is related to the polarisibilities of the elements from 1 and 2.  $\rho_{N1}$  and  $\rho_{N2}$  are the number densities of such elements in phase 1 and in phase 2 respectively. The interaction energy between a column of unit cross section of phase 1 and the entire phase 2 is obtained by integration of  $u_{1,phase2}$  over  $x$  from  $D$  to  $\infty$ .

$$\begin{aligned}
 u_{total} &= \int_D^\infty u_{1,phase2}\rho_{N1}dx = \int_h^\infty -\frac{\pi\beta_{12}\rho_{N2}\rho_{N1}}{6} \frac{1}{x^3} dx \\
 &= -\frac{\pi\beta_{12}\rho_{N2}\rho_{N1}}{12D^2}
 \end{aligned} \tag{S2}$$

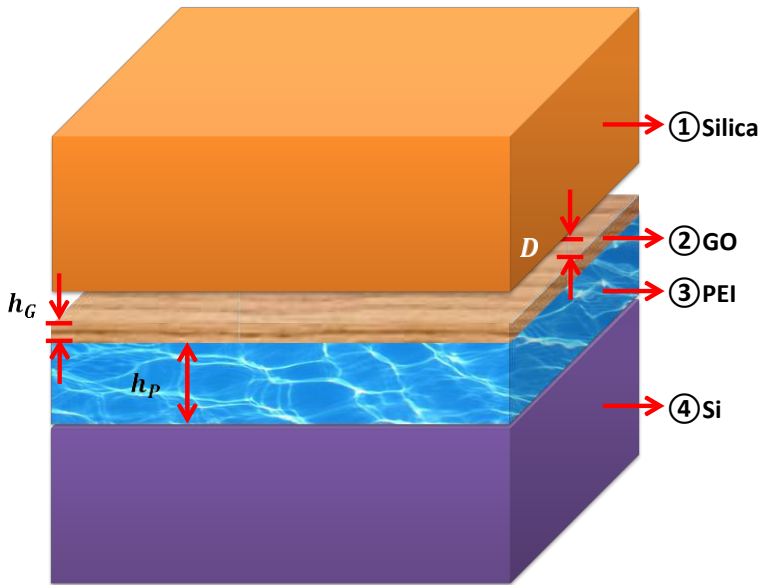


Fig S2. Schematic structure of a silica surface at distance  $D$  from a Si/PEI/GO surface.

In our experiment, we are measuring the interaction between a silica surface and a silicon<sup>1</sup> surface covered by a layer of the polymer PEI and GO (indicated by Si/PEI/GO) as shown in fig. S2. The VdW interaction between a single element of phase 1 and phase 2-4 is described as follows, where  $D$  is the distance between the two flat surface,  $h_G$  is the thickness of GO and  $h_P$  is the thickness of the PEI layer.

$$\begin{aligned}
 u_{1,phase2} &= -\left[ \int_x^{x+h_G} \int_0^\infty \frac{\beta_{12} \pi \rho_{N2} R^2 (d \tan \theta^2)}{r} dR + \int_{x+h_G}^{x+h_G+h_P} \int_0^\infty \frac{\beta_{13} \pi \rho_{N3} R^2 (d \tan \theta^2)}{r} dR \right. \\
 &+ \left. \int_{x+h_G+h_P}^\infty \int_0^\infty \frac{\beta_{14} \pi \rho_{N4} R^2 (d \tan \theta^2)}{r^6} dR \right] \\
 &= -\left[ \pi \beta_{12} \rho_{N2} \int_x^{x+h_G} \int_0^\infty \frac{d(\tan \theta^2) dR}{R^4 (\tan \theta^2 + 1)^3} \right. \\
 &\quad + \pi \beta_{13} \rho_{N3} \int_{x+h_G}^{x+h_G+h_P} \int_0^\infty \frac{d(\tan \theta^2) dR}{R^4 (\tan \theta^2 + 1)^3} \\
 &\quad \left. + \pi \beta_{14} \rho_{N4} \int_{x+h_G+h_P}^\infty \int_0^\infty \frac{d(\tan \theta^2) dR}{R^4 (\tan \theta^2 + 1)^3} \right] \\
 &= -\left[ \frac{\pi \beta_{12} \rho_{N2}}{6} \left( \frac{1}{x} - \frac{1}{(x+h_G)} \right) + \frac{\pi \beta_{13} \rho_{N3}}{6} \left( \frac{1}{(x+h_G)} - \frac{1}{(x+h_G+h_P)} \right) \right. \\
 &\quad \left. + \frac{\pi \beta_{14} \rho_{N4}}{6} \left( \frac{1}{(x+h_G+h_P)} \right) \right] \tag{S3}
 \end{aligned}$$

The interaction energy between a column of unit cross section of phase 1 and the entire phase 2-4 is obtained by integration of  $u_{1,phase2}$  over  $x$  from  $D$  to  $\infty$ .

$$\begin{aligned}
 U(D) &= \int_D^{-\infty} u_{1,phase2} \rho_{N1} dx \\
 &= -\left[ \frac{\pi \beta_{12} \rho_{N2} \rho_{N1}}{12} \left( \frac{1}{D^2} - \frac{1}{(D+h_G)^2} \right) + \frac{\pi \beta_{13} \rho_{N3} \rho_{N1}}{12} \left( \frac{1}{(D+h_G)^2} - \frac{1}{(D+h_G+h_P)^2} \right) \right]
 \end{aligned}$$

<sup>1</sup>In fact the substrate is Silicon covered by a thin native Silica layer. We are in our paper interested in the difference between the interaction with areas where there is a monolayer of GO on the outside and areas where anyway. Therefor we will not spend attention to its actual detailed structure. The fact that also the AFM tip consists of Silicon covered by a native Silica layer will be addressed in the next section.

there is a bilayer of GO on the outside. In this difference the contributions due to the substrate cancel out

anyway. Therefore we will not spend attention to its actual detailed structure. The fact that also the AFM tip consists of Silicon covered by a native Silica layer will be addressed in the next section.

$$+ \frac{\pi\beta_{14}\rho_{N4}\rho_{N1}}{12} \left( \frac{1}{(D + h_G + h_p)^2} \right)] \quad (S4)$$

The Hamaker constant between phase 1 and phase 2 is defined as:  $A_{12} = \pi^2\beta_{12}\rho_{N1}\rho_{N2}$ ,

according to the Berhelot principle<sup>[2]</sup>,  $A_{12} \approx \sqrt{A_{11}A_{22}}$ ,

$$U(D) = -\left[ \frac{A_{12}}{12\pi} \left( \frac{1}{D^2} - \frac{1}{(D + h_G)^2} \right) + \frac{A_{13}}{12\pi} \left( \frac{1}{(D + h_G)^2} - \frac{1}{(D + h_G + h_p)^2} \right) + \frac{A}{12\pi} \left( \frac{1}{(D + h_G + h_p)^2} \right) \right] \quad (S5)$$

## 2. Contribution of Si in the total VdW energy between GO and Si surface with native silica layer

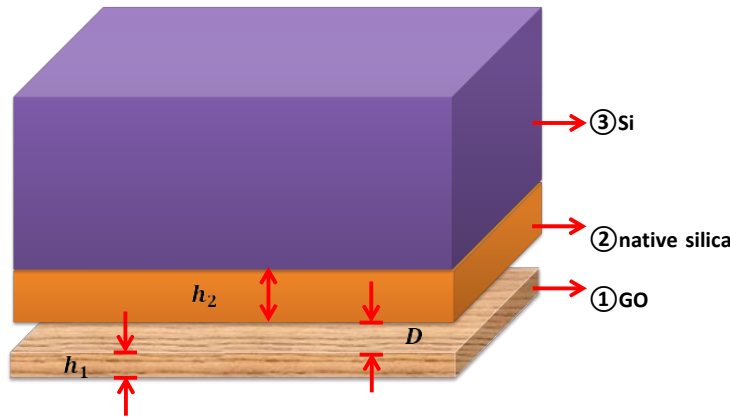


Fig S3. Schematic structure of a GO surface below a Si surface with native silica oxidized layer at distance  $D$ .

The AFM tip consists of Si (labelled by subscript 3 in subsequent equations) covered by a native oxide layer (Silica, Sa, labelled by subscript 2 in subsequent equations). According to Equation (S3), the VdW interaction between a single element of phase 1 and a phase 3 coated by a layer of 2 ( Si coated by Sa) is given by.

$$\frac{\pi\beta_{12}\rho_{N2}}{x^3} - \frac{1}{x^3} - \frac{\pi\beta_{13}\rho_{N3}}{x^3} - \frac{1}{x^3}$$

$$u_{1,phase23} = -\left[ \frac{1}{6} (x+h_2)^2 + \frac{1}{6} (x+h_2)^3 \right]$$

where  $D$  is the distance between the two flat surfaces, and  $h_2$  is the thickness of the native silica layer. The interaction energy between a column of unit cross section of phase 1 and the phase 3 coated by a layer of 2 is obtained by integration of  $u_{1,\text{phase}23}$  over  $x$  from  $D$  to  $D + h_1$ , where  $h_1$  is the thickness of GO.

$$\begin{aligned}
 U(D) &= \int_D^{D+h_{GO}} u_{1,\text{phase}23} \rho_{N1} dx \\
 &= - \left\{ \frac{\pi \beta_{12} \rho_{N2} \rho_{N1}}{12} \left[ \left( \frac{1}{D^2} - \frac{1}{(D+h_1)^2} \right) - \left( \frac{1}{(D+h_2)^2} - \frac{1}{(D+h_2+h_1)^2} \right) \right] \right. \\
 &\quad \left. + \frac{\pi \beta_{13} \rho_{N3} \rho_{N1}}{12} \left( \frac{1}{(D+h_2)^2} - \frac{1}{(D+h_2+h_1)^2} \right) \right\} \\
 &= - \left\{ \frac{A_{12}}{12\pi} \left[ \left( \frac{1}{D^2} - \frac{1}{(D+h_1)^2} \right) - \left( \frac{1}{(D+h_2)^2} - \frac{1}{(D+h_2+h_1)^2} \right) \right] \right. \\
 &\quad \left. + \frac{A_{13}}{12\pi} \left( \frac{1}{(D+h_2)^2} - \frac{1}{(D+h_2+h_1)^2} \right) \right\} \\
 &= -(mA_{12} + nA_{13}) \tag{S7}
 \end{aligned}$$

Where  $A_{12} = \pi^2 \beta_{12} \rho_{N1} \rho_{N2}$  and  $A_{13} = \pi^2 \beta_{13} \rho_{N1} \rho_{N3}$ . The parameters  $m$  and  $n$  quantify the contributions to the total VdW interaction of the silica layer and of bulk silicon, respectively.

Using reasonable values  $D = h_1 = 0.9 \text{ nm}$  and  $h_2 = 2 \text{ nm}$ , we find that  $U(D) \approx 17A_{12} + A_{13}$ . So, the contribution of Si is relatively small and thus we neglect the effect of Si. Fig S4 shows the ratio  $m/n$  of the contributions from the silica layer and bulk Si in the total VdW energy as a function of separation distance  $D$ , as calculated using Equation (S7). We see that neglecting Si becomes more accurate at small  $D$ , where the total VdW energy increases rapidly. When the surface separation distance  $D$  is small and VdW interaction is strong, the error is very small (<0.5%). When  $D$  increased to 1.5 nm, where the VdW interaction is 300 times decreased, the error is still less than 20%.



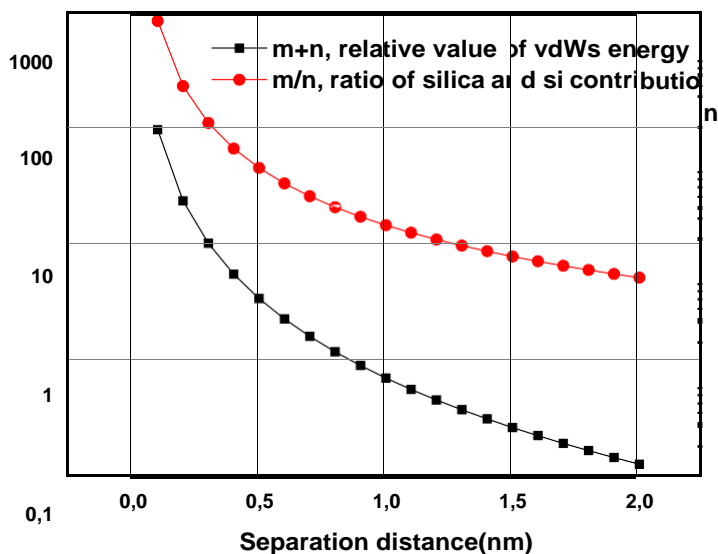
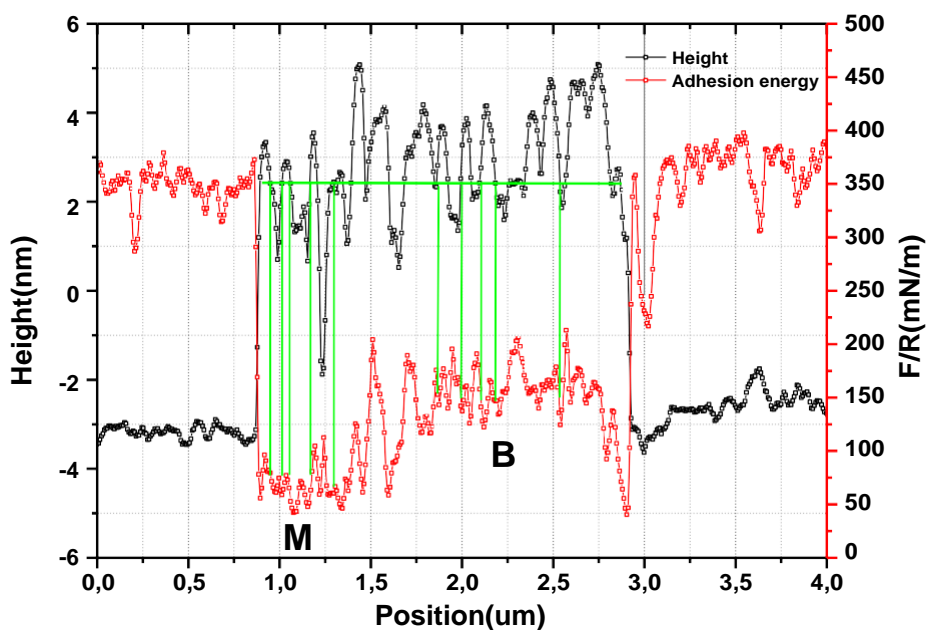


Fig S4. Evaluate the contribution from native silica layer and bulk silicon in the total VdW energy between GO and Si surface with 2 nm thick native oxidized silica layer.

### 3. Determination of the normalized adhesion force



1  
2  
3  
4  
5  
6  
7  
8  
9  
10  
11  
12  
13  
14  
15  
16  
17  
18  
19  
20  
21  
22  
23  
24  
25  
26  
27  
28  
29  
30  
31  
32  
33  
34  
35  
36  
37  
38  
39  
40  
41  
42  
43  
44  
45  
46  
47  
48  
49  
50  
51  
52  
53  
54  
55  
56  
57  
58  
59  
60  
61  
62  
63  
64  
65

Figure S5. Illustration of the selection of measuring locations from the normalized force image of Fig. 3c.

As explained in our letter's main text, and illustrated in Fig. 1a and 1b, in order to obtain the interaction between the AFM tip and the bottom layer of a GO bilayer we need to measure the adhesion force between the AFM tip and the Si/PEI/GO monolayer and between the AFM tip and Si/PEI/GO bilayer. Moreover, it is required that the thicknesses of the PEI/GO films at which these adhesion forces are measured are the same. The Hybrid Mode AFM method enables us to select Si/PEI/GO monolayer locations and Si/PEI/GO bilayer locations where the height is the same. Moreover, with this method the adhesion-force values at these locations are readily available. In Fig. S5, we see that there are considerable variations in the height of PEI/GO monolayer regions and PEI/GO bilayer regions, with an amplitude of about 2 nm. However, it is recognised as well that there are PEI/GO monolayer regions (marked as M) and PEI/GO bilayer regions (marked as B) with similar height. Observe the regions where the height coincides with the green horizontal line. Ten locations are chosen; half of them are at a PEI/GO monolayer and the other half at PEI/GO bilayer. Thus, we have five separate experiments with the same situation as illustrated in Fig. 1a and 1b. The normalized adhesion force is  $76 \pm 3 \text{ mN/m}$  at the PEI/GO monolayer, and  $151 \pm 4 \text{ mN/m}$  at the PEI/GO bilayer. The difference is  $75 \pm 5 \text{ mN/m}$ .

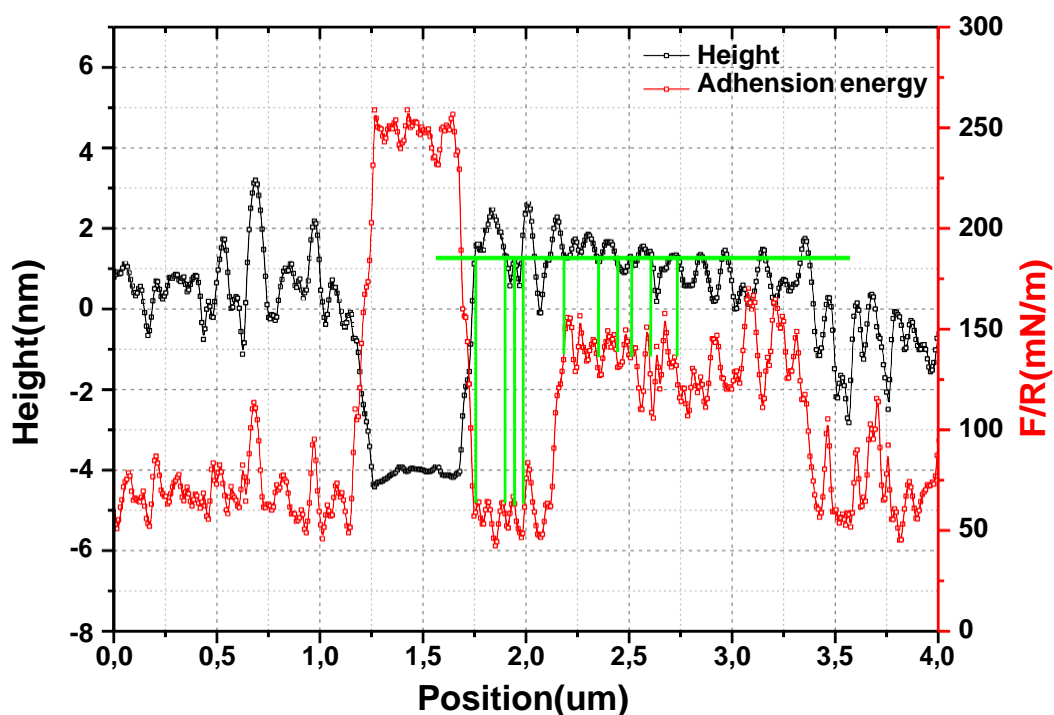


Figure S6. Illustration of the selection of measuring locations from the normalized force image of Fig. 3f.

The same approach to select measuring locations, was used for the repeated experiment (Fig. 3f, S6). Four PEI/GO monolayer locations were selected. There the normalized adhesion force was  $63 \pm 2 \text{ mN/m}$ . Six locations are selected at PEI/GO bilayer, at which the normalized adhesion force was  $136 \pm 3 \text{ mN/m}$ . The difference between these values is  $73 \pm 4 \text{ mN/m}$ . That this is the same, within experimental error, as with the first experiment, even though the separate forces at the monolayer and at the bilayer are different from the first experiment, confirms the soundness of our approach.

4. Determination of the thickness of a single GO nanosheet

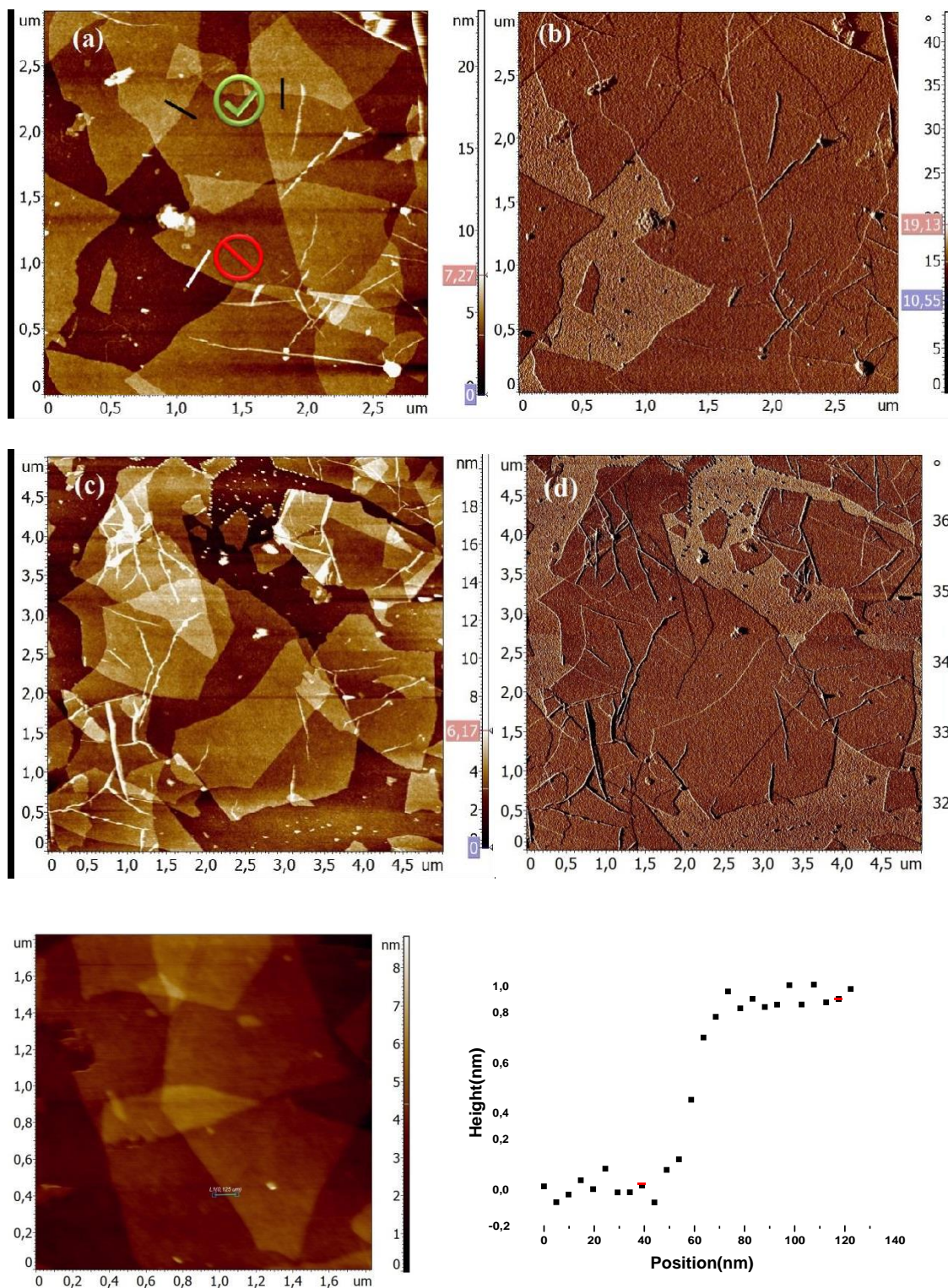


Figure S7. Measuring the thickness of a GO nanosheet. (a) and (c) show the height image at different locations of the Si/PEI/GO sample obtained by tapping mode AFM. The sample has a similar structure as illustrated in Fig 2.2. The black lines in (a) show the data selection,

1 where 2 GO layers overlapped. The white line in (a) shows the location that is not taken into  
2 account, where GO is on top of PEI. (b) and (d) are the AFM phase images corresponding  
3 with (a) and (b), respectively.<sup>[3]</sup> The PEI/GO patch and bare PEI patch can be easily  
4 differentiated from the phase images. (e) Height image obtained by contact mode AFM. (f)  
5 typical height profile from the height image (e).<sup>[4]</sup>  
6  
7  
8  
9

10 The thickness of a GO layer is determined as shown in Fig. S7. Fig S7.a and c show height  
11 images obtained by tapping mode AFM at different locations of a Si/PEI/GO sample with a  
12 similar structure as illustrated in Fig 2.2. In the phase image we recognize PEI patches and  
13 GO monolayer- or bilayer patches. The thickness of the upper layer of the GO bilayer was  
14 measured, by measuring the height difference along the edge between bilayer and monolayer,  
15 as marked by black lines in S7.a. Fig S7.e shows the height image obtained using contact  
16 mode AFM, the applied force is similar as used in Hybrid mode AFM scanning.  
17  
18  
19  
20  
21  
22  
23  
24  
25  
26  
27

28 The average thickness of the GO upper layer of a PEI/GO bilayer patch measured over 30  
29 points by means of tapping mode AFM is  $0.97 \pm 0.08 \text{ nm}$ . The average thickness of the GO  
30 upper layer measured over 10 points using contact mode is  $0.89 \pm 0.06 \text{ nm}$ . In Hybrid mode  
31 scanning, the AFM tip contacts with the surface. Thus, the later one was used to calculate the  
32 Hamaker constant here.  
33  
34  
35  
36  
37  
38  
39  
40  
41  
42  
43  
44  
45  
46  
47  
48  
49  
50  
51  
52  
53  
54  
55  
56  
57  
58  
59  
60  
61  
62  
63  
64  
65

## 5. Characterization of GO

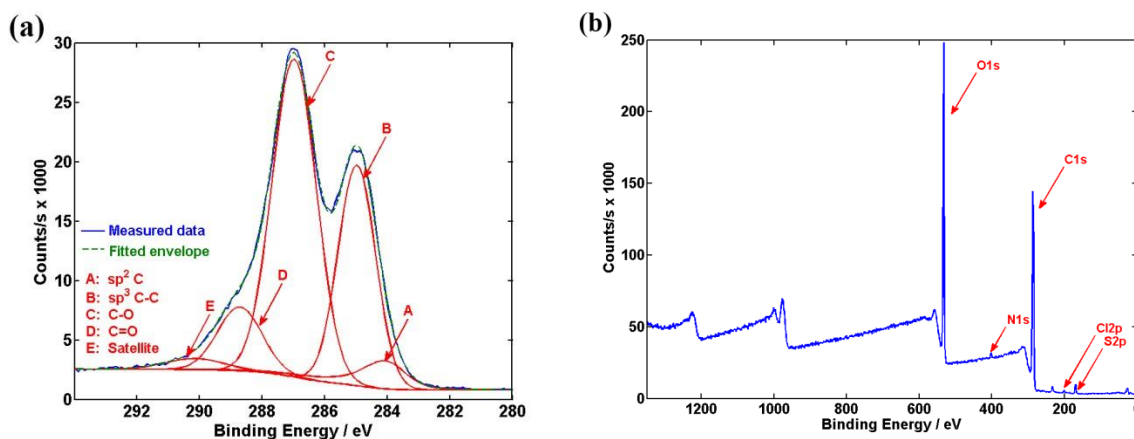


Figure S8. (a) High resolution C-1s-XPS spectrum of GO, and deconvoluted curves

corresponding to C-C, C-O, and C=O moieties. (b) Survey spectrum of GO.

X-ray photoelectron spectroscopy (XPS) was used to characterise the elemental composition of the GO powder as received.<sup>[5]</sup> The C-1s-XPS spectrum of the GO is shown in Fig. S8, with the deconvoluted fitting curves. From the ratio of the peak areas, the molar ratio of C=O to C-O moieties is about 1:5. The atomic fraction of C and O is 67.5% and 30.4%, respectively.

Besides C and O, XPS also revealed that the presence of S (1.6%) and Cl (0.6%), which must have been introduced into GO during manufacturing.

This elemental analysis was carried out using an X-ray Photoelectron Spectrometer (XPS, *Thermo Fisher Scientific, K Alpha* model). A monochromated Al K $\alpha$  X-ray source was used.

XPS measurements were taken in normal emission with a spot size of 100  $\mu\text{m}$  at a base pressure of  $10^{-8}$  mbar. During all XPS measurements, the flood gun was enabled to compensate for the potential charging of surfaces. Survey spectra and elemental region scans were taken at pass energy of 200 eV and 50 eV respectively and averaged over 10 scans. The spectra were analyzed using *Avantage* processing software. The XPS spectra were background corrected using the “Smart” base line function available in the software, and peak fitting was done using the Simplex peak fitting algorithm with a Gaussian (70%) – Lorentzian (30%) convolution function.

## 6. Determine the AFM tip radius using High-resolution SEM

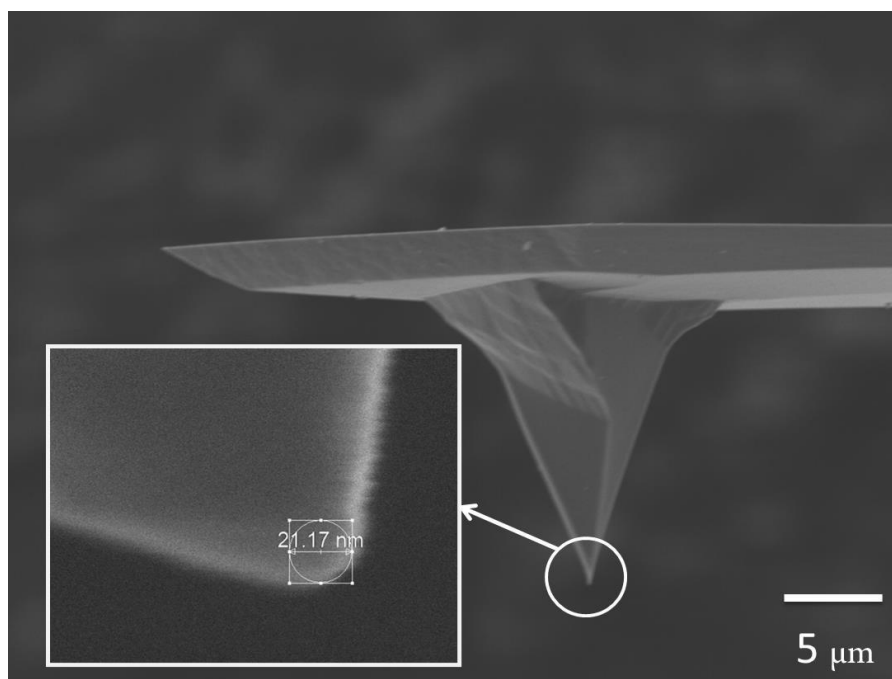


Figure S9. High-resolution SEM image of the AFM tip.

The Nova NanoSEM™ scanning electron microscope (SEM) was used to characterize the radius of the AFM tip. The radius of the AFM tip is determined as 10.6 nm. The AFM chip was glued on the substrate with its side face perpendicular to the substrate. The over view of the tip is recorded, at magnification of 3,500 (operated at 5 kV). The inset image is the high-resolution image of the tip, obtained at magnification of 650,000 (operated at 10 kV).

## 7. Calculation of the Hamaker constant between GO and silica

According to Equation (5),  $A_{SG} = 8d^2 \frac{\Delta F}{R} + \sqrt{A_{SS}A_{PP}}$ , herein,  $d = 0.89 \pm 0.06 \text{ nm}$ ,  $A_{SS} = 16.09 k_B T$ ,  $A_{PP} = 13 \pm 3 k_B T$ . As shown in part 6, the tip radius is 10.6 nm. In the Hybrid mode AFM, the tip radius was set as 10 nm, thus, the  $\frac{\Delta F}{R}$  is modified as  $70.75 \pm 4.7 \text{ mN/m}$ .

$A_{SG}$  was calculated as  $124.6 k_B T$ . According to the definition of error, the standard error for

$A_{SG}$  is

$$\sigma_{A_{SG}} = \sqrt{\left(\frac{\partial A_{SG}}{\partial \frac{\Delta F}{R}}\right)^2 \sigma_{\frac{\Delta F}{R}}^2 + \left(\frac{\partial A_{SG}}{\partial d}\right)^2 \sigma_d^2 + \left(\frac{\partial A_{SG}}{\partial A_{SP}}\right)^2 \sigma_{A_{SP}}^2} = 16.6 k_B T.$$

Thus, the Hamaker constant between GO and silica is determined as  $124.6 \pm 16.6 k_B T$ .

## References

- [1] J. Visser, *Advances in Colloid and Interface Science* 1972, 3, 331.
- [2] J. Lyklema, 1991.
- [3] R. S. McLean, B. B. Sauer, *Macromolecules* 1997, 30, 8314; J. Tamayo, R. Garcia, *Langmuir* 1996, 12, 4430.
- [4] I. Schmitz, M. Schreiner, G. Friedbacher, M. Grasserbauer, *Analytical chemistry* 1997, 69, 1012.
- [5] S. C. Lee, S. Some, S. W. Kim, S. J. Kim, J. Seo, J. Lee, T. Lee, J.-H. Ahn, H.-J. Choi, S. C. Jun, *Scientific reports* 2015, 5.